Available online at www.sciencedirect.com

ScienceDirect

Energy Procedia 35 (2013) 113 – 120

Energy Procedia

Deep Wind, 24-25 January 2013, Trondheim, NORWAY

Perturbation in the atmospheric acoustic field from a large offshore wind farm in the presence of surface gravity waves

Mostafa Bakhoday Paskyabi*

Geophysical Institute, University of Bergen, Allégaten 70, N-5007 Bergen, Norway

Abstract

In this study a quantitatively reliable approximation of atmospheric sound wave propagation is given in the presence of a large wind farm. Rough sea surface is used as lower boundary condition at the sea surface, and an acoustic point source located at the left corner of computational domain is used to generate cylindrical symmetric sound waves. A stable finite difference approach is applied to achieve high–resolution and accurate results while maintaining efficiency of computations. A series of test cases is conducted to demonstrate the variability of acoustic wave field when accounting the effects of surface gravity waves and wind farm. Although results provide good insights into the sound wave structure in this complex waveguide, they suggest that there are some important physical processes such as range–dependent structure of sound speed and turbulence that should be included into the modeling procedure.

Selection and peer-review under responsibility of SINTEF Energi AS

Keywords: Parabolic equation, atmospheric acoustic wave, Wide–angle parabolic equation, wind farm

1. Introduction

The cost increase of the fossil fuels and global warming issue are resulting in a rapid development of renewable energy sources. Nowadays, wind energy and especially offshore wind farms are one of popular and challenging type of renewable energy resources. Offshore wind farms are often installed on coastal waters and comprising hundreds of wind turbines that affects the noise disturbances patterns in the adjacent coastal regions. Negative impacts of this dynamic ambient noise to the public health motivate to optimize designing of the offshore wind farms under this constraint to reduce public discomfort. Wind farm–induced noise levels are affected by several physical and meteorological factors such as the decaying mechanism away from boundaries, the wave climate changes in development site, meteorological changes, the refraction induced by temporal and spatial variation of sound speed, and the effects of topography. Simulations of atmospheric sound propagation can approximately provide information required to control environmental noise levels.

Parabolic Equation (PE) models have long been used by the underwater acoustics community to study sound propagation because of their less computational efforts than full elliptic wave equation model. Meanwhile, the PE methods have fast convergence within a reasonable cpu–time and memory [1]. While this

*Corresponding author
Email address: Mostafa.Bakhoday@gfi.uib.no (Mostafa Bakhoday Paskyabi)

1876-6102
Selection and peer-review under responsibility of SINTEF Energi AS
doi:10.1016/j.egypro.2013.07.164

technique provides good prediction of acoustic field, the variable topography and boundary complicate the discritization of model, especially in the mixed type boundary condition [2]. Using conformal mappings in order to flatten successive segments of the variable ground topography is an example for overcoming this issue [3].

In this study, stable finite difference discretizations of a wide-angle parabolic equation is used to model long range acoustic sound propagation over a wind farm which acts as an obstacle on the incoming sound wave. The height of wind farm is considerably higher than the sea surface roughness. A series of idealized test cases are conducted to show numerically the perturbations of atmospheric acoustic field as a function of farm height and background profile of sound speed.

The rest of the paper is organized in the following way. First, I establish the relevant PE approximations for atmospheric acoustics using finite difference technique and range marching algorithm. Section 3 includes three test cases relevant to atmospheric acoustic field to demonstrate the effectiveness of numerical techniques. The final section provides a brief summary and discussion.

2. PE model

The PE model used in this study is based on a two–dimensional rz–plane, finite difference, and range marching algorithm [1]. Assuming flat surface condition, the pressure–release boundary condition can be written as, $\psi(r, z = 0) = 0$ by using an image atmosphere assumption. Here, $\psi = \exp(-k_0 r) p r^{1/2}$ is the field function where p is the acoustic pressure, k_0 denotes the reference wavenumber, and r and z are radial range and height, respectively. The field function is extracted from the Helmholtz equation by introducing a pseudo–differential operator $\sqrt{1+X}$, where

$$X = n^2 - 1 + \frac{1}{k_0^2}\frac{\partial^2}{\partial z^2},$$

and is formulated as:

$$\frac{\partial \psi}{\partial r} = ik_0\left(-1 + \sqrt{1+X}\right)\psi, \tag{1}$$

where i is the imaginary unit, $k_0 = 2\pi f/c_0$ is the reference wavenumber associated with the reference sound speed c_0 and acoustic source frequency f, $n(r, z) = c_0/c(r, z)$ is the index of refraction, $c(r, z)$ is the speed of sound in the atmosphere. The Wide–Angle–Parabolic–Equation (WAPE) model is obtained by substituting [1,1] Pade approximation for $\sqrt{1+X}$ given in Eq. (1) as

$$-1 + \sqrt{1+X} = \frac{1/2X}{1 + 1/4X} = \frac{1/2(n^2-1) + 1/2k_0^{-2}\partial_z^2}{1 + 1/4(n^2-1) + 1/4k_0^{-2}\partial_z^2}.$$

Substituting above approximation into the Eq. (1) and using centered finite difference over interval r and $r + \Delta r$ give:

$$\begin{aligned} \frac{\partial \psi}{\partial r} &= \frac{\psi(r+\Delta r, z) - \psi(r, z)}{\Delta r}, \\ \psi(r, z) &\approx \frac{\psi(r+\Delta r, z) + \psi(r, z)}{2}, \end{aligned}$$

Eq. (1) can be rewritten as

$$\left[\frac{4ik_0}{\Delta r} + k_0^2(n^2-1) + \frac{\partial^2}{\partial z^2}\right]\psi(r+\Delta r, z) = \left[\frac{4ik_0}{\Delta r} - k_0^2(n^2-1) - \frac{\partial^2}{\partial z^2}\right]\psi(r, z), \tag{2}$$

The boundary condition at the sea surface is obtained by equaling surface impedance to the ratio between the sound pressure and the normal particle velocity. The upper boundary condition is introduced by using an absorbing layer in the upper region of the computational domain.

To properly model acoustic wave propagation over irregular terrain, the effects of both forward and backward reflected, refracted, and diffracted waves must be very well predicted. To this end, the numerical solution of the PE is achieved by the Green's function PE version of Eq. (1), in which the field is originated from an acoustic source at a reference range and is marched out in the range by computing the vertical sound field at each range step via [3]:

$$\begin{aligned}\psi(r+\triangle r) &= \exp\left(i\frac{\Delta r\delta k^2(z)}{2k_0}\right)\\ &\times\ [\frac{1}{2\pi}\int_{-\infty}^{\infty}[\Psi(r,k')+R(k')\Psi(r,-k')]\times\exp\left(i\Delta r\left(\sqrt{k_0^2-k'^2}-k_0\right)\right)\\ &\times\ 2i\beta\Psi(r,\beta)\times\exp\left(i\Delta r\left(\sqrt{k_0^2-\beta^2}-k_0\right)\right)\exp(-i\beta z)], \end{aligned} \tag{3}$$

where Ψ is the Fourier transform of ψ, $\beta=-k_0/Z_g$ represents the surface wave pole in the reflection coefficient $R(k')$:

$$R(k')=\frac{k'Z_g-k_0}{k'Z_g+k_0}, \tag{4}$$

where Z_g denotes the normalized ground impedance, and $\delta k^2=k^2-k_0^2$ is the vertical wavenumber fluctuation. In Eq. (3), terms $\Psi(r,k')$, $R(k')\Psi(r,-k')$, and $\Psi(r,\beta)$ represent the direct wave, the reflected wave by ground, and the surface wave, respectively [4, 2].

3. Numerical Results

We use a Gaussian function, $\psi(r=0,z)$, as a starting source function:

$$\psi(r=0,z)=\sqrt{k_0}\left[\exp\left(-\frac{k_0}{2}(z-z_s)^2\right)+\frac{Z_g-1}{Z_g+1}\exp\left(-\frac{k_0}{2}(z+z_s)^2\right)\right], \tag{5}$$

where z_s denotes the source height.

We include the effect of refraction using the effective sound speed. An initial logarithmic range–independent sound speed profile is given as

$$c(z)=c_0+a\ln\left(1+\frac{z}{z_0}\right), \tag{6}$$

where a is a refraction constant (here, ≈ 1), and z_0 is the sea surface roughness computed from Charnok relation [5].

The horizontal and vertical step sizes are set to $\Delta r=15\lambda$ and $\Delta z=0.5\lambda$, where λ is the wavelength at the lower boundary. To avoid spurious reflections of sound waves from the upper boundary, we use an artificial absorption layer with thickness of 50λ. For the comparison purposes, the transmission loss is used and defined at point (r,z) by

$$20\log_{10}\left[\frac{|\psi(r,z)|}{|\psi_{z_r}|}\right],$$

where ψ_{z_r} is a reference acoustic field measured at distance z_r from the source (usually $z_r=1$ m).

Test Case 1.

In this test case, the surface elevation is generated by using the Joint North Sea Wave Project (JONSWAP) spectrum [6] in the form

$$S(f_s)=\alpha g^2\omega^{-5}\exp\left[-\frac{5}{4}\left(\frac{f_s}{f_p}\right)^{-4}\right]\gamma^{\delta_0}, \tag{7}$$

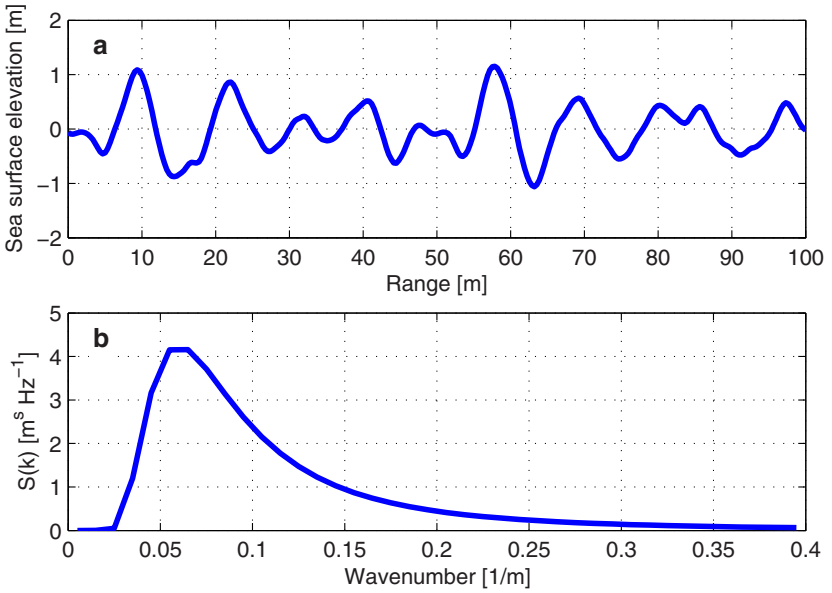

Fig. 1. Example of sea surface realizations generated by empirical model. a) sea surface elevation b) JONSWAP wavenumber spectrum for wind speed of 10 m s^{-1} at a height of 10 m.

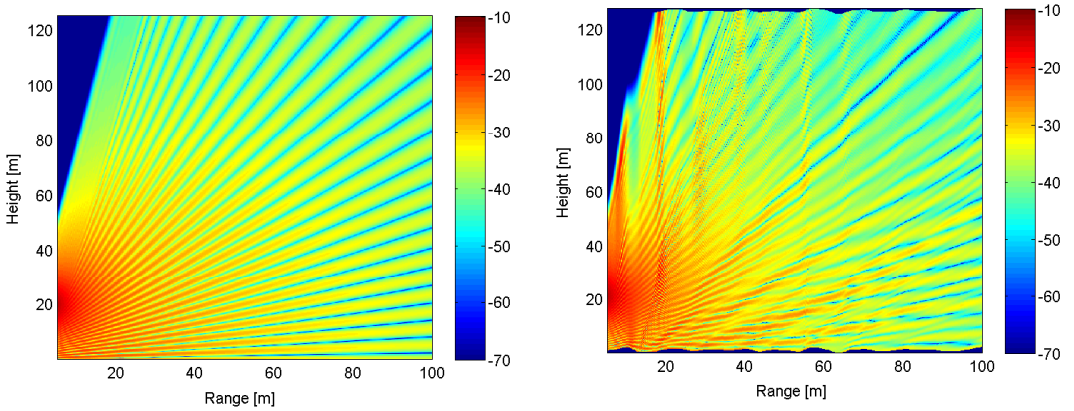

Fig. 2. Transmission loss due to a point source at frequency of 150 Hz at a height of 20 m above the mean sea surface. *left*) without sea surface wave effect, *right*) with sea surface wave effect using GTPE scheme.

where $\omega = 2\pi f$ is the angular frequency, f_s denotes the surface wave frequency in Hz, g is the gravitational acceleration, $\alpha = 0.0509$ is a constant, $\gamma = 3.3$, and δ_0 is a peak enhancement factor given by

$$\delta_0 = \exp\left[-\frac{(f_s - f_p)^2}{2\sigma_0^2 f_p^2}\right],$$

where $\sigma_0 = 0.07$ for $f_s \leq f_p$, and $\sigma_0 = 0.09$ for $f_s > f_p$. Here, f_p is the peak frequency. The spatial variability of surface elevation can be calculated by transforming the wave energy spectrum from frequency space to the wavenumber space (Fig. 1). Figure 2 shows the calculated transmission loss as a function of range and height both to regular and irregular surface using the GFPE scheme. An harmonic point source at frequency of 50 Hz is located at height of 20 m above the mean sea surface. The maximum range of simulation is 100 m. Furthermore, I ideally assume the surface as a hard grass surface, in which the impedance can be estimated as

$$Z_g = 1 + 9.08\left(\frac{f}{\sigma'}\right)^{-0.75} + 11.9i\left(\frac{f}{\sigma'}\right)^{-0.73}, \tag{8}$$

where σ' is the flow resistivity (here, ≈ 500) in Rayls (in SI based units, 1 Ryle=1 kg $s^{-1}m^{-2}$). Note that the GFPE gives an angle restriction for propagation and scatter that leads to unrealistic results in the upper left part of the computational domain.

Figure 2-*left* shows the amplitude of the total field through a regular flat–surface waveguide, due to a Gaussian beam traveling horizontally with principal direction parallel to the mean surface direction. The source is located at the left, and the field vanishes on both surfaces. Fig. 2-*right* illustrates the TL field, when the surface is rough; here the scattering has largely destroyed the deterministic pattern of the corresponding regular case. By comparing Figs. 2-*left* and 2-*right*, we can deduce that the TL field close to the sea surface is sensitive even to small surface elevation.

Test Case 2. In the test case considered here, I take a rectangular domain with height of 300 m, consisting of two fluid layers, separated by a horizontal interface and having sound speeds of 340 and 1700 m/s for air and water layers, respectively. I consider the transmission loss structure for the three different frequencies of 50, 150, and 350 Hz, respectively due to a harmonic source modeled by Gaussian distribution (Eq. 5) at height of 50 m. The wind farm is shown as a dark blue area around 5 km downwind from the start range of calculation with hight of 50 m and a characteristic length of 10 km. The total calculation range is 20 km. Figures 3-*Top:left*, 3-*Middle:left*, and 3-*Bottom:left* show that the acoustic TL field is in a suitable logarithmic scale, when the wind farm effect is not accounted. These figures indicate a similar sound wave propagation structure, since the most significant contributions to the propagation are supported from lower part close to the sea surface. Figures 3-*Top:right*, 3-*Middle:right*, and 3-*Bottom:right* show the distortions brought upon by the presence of wind farm. By comparing figures without (NF) and with farm (WF) effects, it can be inferred that the wind farm acts as a drag element on the sound field up till its height (here 50 m), and the resulting acoustic field is sensitive to its presence.

Test Case 3. In order to further examine the transmission loss variation created by a wind farm, the model is run using GFPE scheme for a sound field produced by a harmonic acoustic source at frequencies of 50 and 100 Hz, respectively with a logarithmic sound speed profile, in which $c_0 = 342$ m s^{-1} and $a = 1$ (Eq. 6). Figure 4 shows a comparison of predicted TL relative to the microphone at different heights, i.e. 50, 100, and 150 m above the mean sea level. Other model configurations are the same as those used in the second test case. At the microphone height of 50 m, the simulated sound field at the lowest frequency, 50 Hz, decreases by approximately 12-20 dB at region of farm (Figs. 4 Top:*left*, and *right*). At the higher highes, 100 and 150 m, the levels are relatively constant and less–dependent to the farm induced anomalies. For the source at frequency of 100 Hz, Figs. 4 Bottom:*left* and *right*) offer decreasing of TL in the presence of wind farm by approximately 2-13 dB.

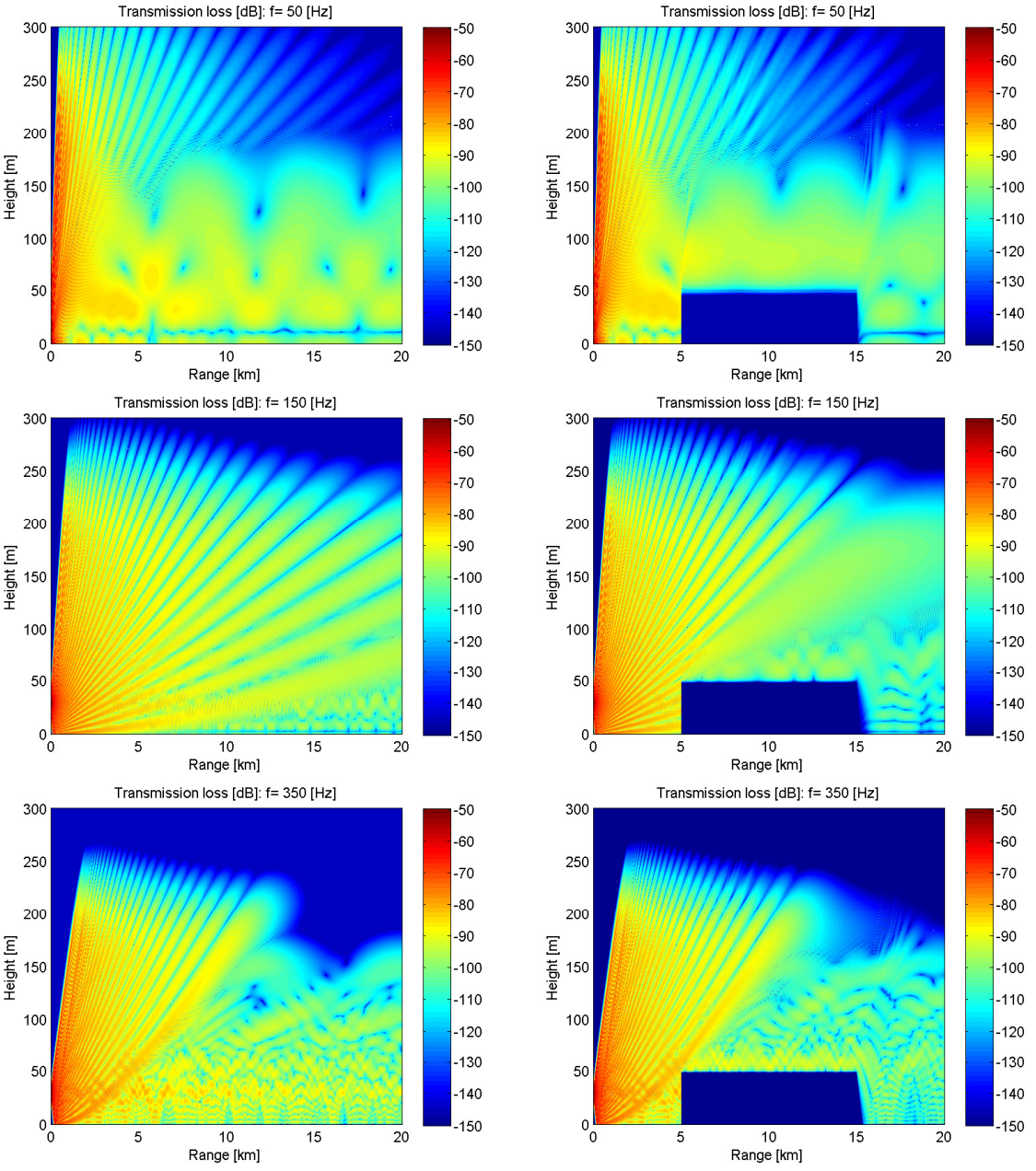

Fig. 3. Transmission loss due to a point source with different frequencies at a height of 50 m above the mean sea surface. The WAPE is applied to produce acoustic wave field. *Top:left*) without wind farm effect for a 50 Hz acoustic point source, *Top:right*) with including a wind farm located at 5 km away from the start of computational domain with height of 50 m and characteristic length of 10 km. An acoustic point source is located at 50 m above the mean sea surface, *Middle:left*) without wind farm effect for a 150 Hz acoustic point source, *Middle:right*) with wind farm effect for a 150 Hz acoustic point source, *Bottom:left*) without wind farm effect for a 350 Hz acoustic point source, and *Bottom:right*) with wind farm effect for a 350 Hz acoustic point source.

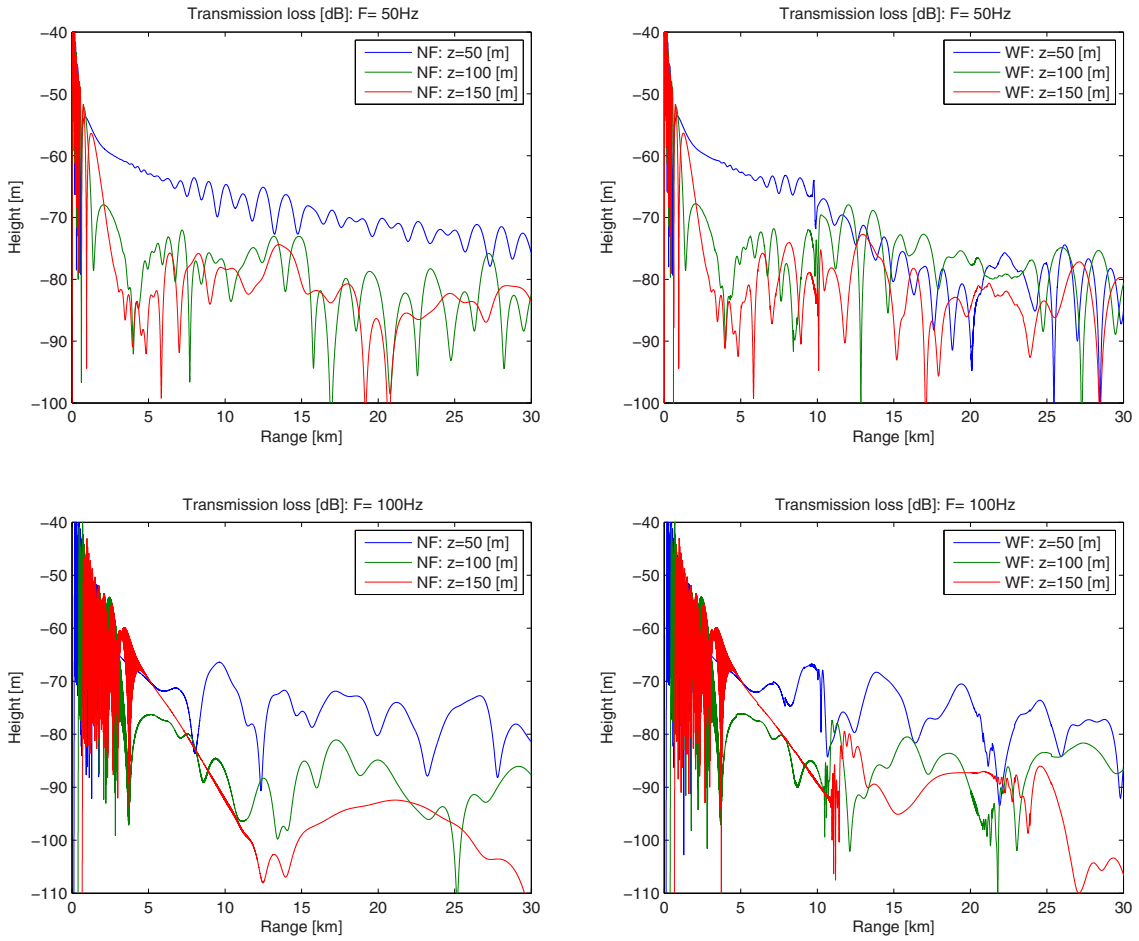

Fig. 4. Comparison of transmission loss prediction using GFPE versus range for acoustic source at height of 50 m and different receiver height. *Top:left*) propagation without farm (NF) effect for point source at frequency of $F = 50$ Hz and heights of 50, 150, and 350 m, respectively, *Top:right*) propagation with farm (WF) effect for point source at frequency of $F = 50$ Hz and heights of 50, 150, and 350 m, respectively, *Bottom:left*) propagation without farm effect for point source at frequency of 100 Hz and heights of 50, 150, and 350 m, respectively, and *Bottom:right*) propagation with farm effect for point source at frequency of 100 Hz and heights of 50, 150, and 350 m, respectively.

4. Summary

A series of test cases were conducted to study the acoustic pressure field variation with and without farm and surface gravity wave effects using WAPE and GFPE models. The empirical JONSWAP model was used to provide sea surface elevation information. The numerical results properly predicted the variation of TL and followed the expected physical behavior of acoustic waveguide when a large wind farm imposed into the acoustic waveguide and in the presence of rough sea surface. Although, using WAPE and GFPE offered good insights into the variability of acoustic sound wave propagation, the presented schemes to include efficiently the wind farm effect on the acoustic field require further investigations on parameterizing sea surface impedance (here, I used ideally hard grass impedance), sea surface aerodynamic roughness length, effects of turbulence, and some other excluded environmental and theoretical factors. Furthermore, to confirm skills of different numerical techniques, the long term off–shore measurements of acoustic field is required together with measurements of the meteorological conditions and surface gravity waves, surface drifts, and near–surface currents.

5. Acknowledgements

This work has been performed under the Norwegian Center for Offshore Wind Energy (NORCOWE). Furthermore, I would like to thank Dr. Roland Kruse for using his PE code to develop my numerical scheme.

References

[1] M. Bakhoday-Paskyabi, F. Rashidi, Wide angle parabolic equation based on one–periodic Daubechies wavelet for modelling underwater wave propagation, WSEAS Trans. On Math. 4 (2005) 204–211.
[2] E. M. Salomons, Caustic diffraction fields in a downward refracting atmosphere, J. Acoust. Soc. Am. 104 (6) (1998) 3259–3272.
[3] R. A. Sack, M. West, A parabolic equation for sound propagation in two dimensions over any smooth terrain profile: the generalised terrain parabolic equation (GT–PE), Appl.Acoust. 45 (1995) 113–129.
[4] E. M. Salomons, Computational atmospheric acoustics, Kluwer Academic Publishers, 2001.
[5] H. Charnock, Wind stress on a water surface, Quart. J. Roy. Meteor. Soc. 81 (1955) 639–640.
[6] L. H. Holthuijsen, Waves in Oceanic and Coastal Waters, Cambridge University Press, 2007.